FIRST-PRINCIPLES STUDY ON THE MECHANICAL PROPERTIES OF $Al_{1-x}TM_xP$

by

Ai-Feng JIANG and Yu CHEN *

School of Science, Inner Mongolia University of Technology, Hohhot, China

Original scientific paper
https://doi.org/10.2298/TSCI2403277J

Using first-principles calculations, the mechanical properties of orthorhombic phase $Al_{1-x}TM_xP$ (x = 0.0625, 0.125, 0.25; TM = Sc, Ti, V, Cr, Mn, Fe, Co, Ni, Cu, and Zn) crystals were studied. By analyzing the mechanical stability, it was found that $Al_{0.75}Zn_{0.25}P$ is mechanical unstable, and the rest all mechanical stable. The mechanical properties of $Al_{1-x}TM_xP$ were studied, including Bulk modulus, shear modulus, Young's modulus, Poisson's ration, ductility, Vickers hardness, and elastic anisotropy. It was found that $Al_{0.75}Ni_{0.25}P$ has the largest Bulk modulus, the largest Poisson's ratio. $Al_{0.75}Ni_{0.25}P$ has the smallest shear modulus, the smallest Young's modulus and the smallest Vickers hardness. The $Al_{0.75}Ni_{0.25}P$ has the best ductility. $Al_{0.75}Ni_{0.25}P$ and $Al_{0.75}Cu_{0.25}P$ show strong elastic anisotropy, and the $Al_{0.75}Cu_{0.25}P$ has the largest elastic anisotropy. Through the study of the mechanical properties of $Al_{1-x}TM_xP$, it was found that doping Ni into AlP is an effective means to tune its mechanical properties.

Key words: *first-principles, mechanical stability, elastic modulus, Vickers hardness*

Introduction

Aluminum Phosphide (AlP) is an important III-Vcompound semiconductor material, which has been widely applied to functional materials [1, 2]. Doping transition metals into AlP is an effective method to improve its mechanical, magnetic, and optical properties [3-8]. Especially, 2-D AlP materials have more excellent and novel mechanical, magnetic and optical properties [9, 10]. After doping Mn or Cr into AlP, $Al_{1-x}Mn_xP$ and $Al_{1-x}Cr_xP$ have good magnetic properties with Curie temperature of above 300 K [11, 12]. After doping Mn into AlP, the shear modulus and Young's modulus of $Al_{0.75}Mn_{0.25}P$ are less than those of AlP, but the Poisson's ratio and ductility are higher than those of AlP [13]. After doping Mn into AlP, $Al_{0.875}Mn_{0.125}P$ has an absorption peak in the visible light range, and the characteristics of the absorption peak can be controlled by strain [11]. There are many studies on the magnetic and optical properties of semiconductor $Al_{1-x}TM_xP$ (herby TM presents transition metal, rare earth, or non-metal), but few studies on its mechanical properties. In this work, the mechanical properties of $Al_{1-x}TM_xP$ were systematically studied by doping transition metals into AlP, and the effects of transition metal element types and doping concentrations on the mechanical properties of $Al_{1-x}TM_xP$ were studied.

* Corresponding author, e-mail: chenyu@imut.edu.cn

Computational methods

In this work, the first-principles calculation [14-16] is used to study the properties of $Al_{1-x}TM_xP$ (TM = Sc, Ti, V, Cr, Mn, Fe, Co, Ni, Cu, Zn; x = 0.0625, 0.125, 0.25) through the density functional theory (DFT) [17] using a plane-wave pseudopotential method as implemented in the Cambridge Sequential Total Energy Package (CASTEP) code [18, 19]. The Generalized Gradient Approximation (GGA) [20] within the Perdew, Burke, and Ernzerhof (PBE) scheme [21] is used to obtain the exchange-correlation potential. To ensure calculation precision, we employ the plane-wave energy cutoff of 400 eV, and the Brillouin-zone sampling mesh parameters for the k-point set of 2×2×5. The other parameters use the default settings of ultra-fine accuracy.

The zinc blende (*zb*) AlP with space group *F*-43*m* has an experimental lattice constant of 0.5421 nm, the Al an P atom in which are located at positions (0,0,0) and (0.25,0.25,0.25), respectively. In this work, $Al_{0.9375}TM_{0.0625}P$ compound were obtained by substituting one Al atom with one TM atom in a 1×1×1 $Al_3TM_1P_4$ supercell models as shown in fig. 1(a). The $Al_{0.875}TM_{0.125}P$ compound were obtained by substituting one Al atom with one TM atom in a 2×1×1 $Al_7TM_1P_8$ supercell models as shown in fig. 1(b). The $Al_{0.75}TM_{0.25}P$ compound were obtained by substituting one Al atom with one TM atom in a 1×1×1 $Al_{15}TM_1P_{16}$ supercell models as shown in fig. 1(c).

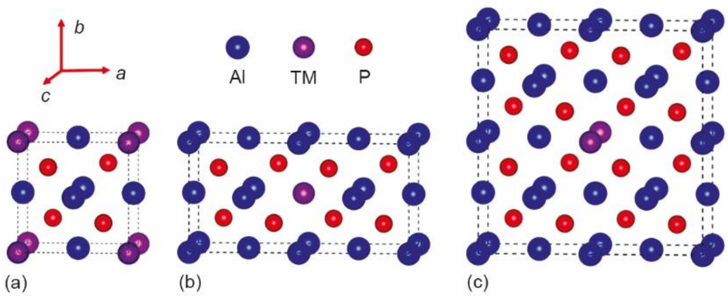

Figure 1. (a) The supercell models of $Al_{0.9375}TM_{0.0625}P$, (b) the supercell models of $Al_{0.875}TM_{0.125}P$, and (c) the supercell models of $Al_{0.75}TM_{0.25}P$

Results and discussion

Elastic constants and mechanical stability

Elastic constants of crystals provide a link between mechanical and dynamical behaviors, they are also important information concerning the elastic response of a crystal to an external pressure. Elastic constants are important parameters to describe mechanical properties of solids. This elastic matrix has size 6×6 and it is symmetric. The elastic constants, C_{ij}, for orthorhombic $Al_{1-x}TM_xP$ supercell predicated by GGA method. According to the elastic constants, it is found that $Al_{1-x}TM_xP$ belongs to orthorhombic crystal. The mechanical stabilities of crystal structure under isotropic pressure can be determined by the criteria of independent elastic constants, C_{ij}. For an orthorhombic crystal, there independent components as shown in the following equation [22, 23]:

$$\begin{gathered}C_{ii} > 0 \\ C_{11} + C_{22} - 2C_{12} > 0 \\ C_{11} + C_{33} - 2C_{13} > 0 \\ C_{22} + C_{33} - 2C_{23} > 0 \\ C_{11} + C_{22} + C_{33} + 2(C_{12} + C_{13} + C_{23}) > 0\end{gathered} \tag{1}$$

According to the criteria, except for $Al_{0.75}Zn_{0.25}P$, all $Al_{1-x}TM_xP$ is mechanically stable at ambient pressure. Therefore, $Al_{0.75}Zn_{0.25}P$ will not be studied when studying the mechanical properties of $Al_{1-x}TM_xP$.

Elastic modulus

The elastic modulus of polycrystalline is interconnected to the elastic constants of single crystals. Generally speaking, elastic properties of polycrystalline have greater practical significance than single crystal. Polycrystalline elastic properties are properties by bulk modulus, B, shear modulus, G, Young's modulus, E, and Poisson's ration, μ. There are two models to evaluate the modulus: the Voigt method and Reuss method, which provide the upper and lower bounds of the polycrystalline elastic modulus, respectively. For different crystalline systems, the bulk modulus and shear modulus according to Voigt can be expressed [24, 25]:

$$B_{\mathrm{v}} = \frac{C_{11} + C_{22} + C_{33} + 2(C_{12} + C_{13} + C_{23})}{9} \tag{2}$$

$$G_{\mathrm{v}} = \frac{C_{11} + C_{22} + C_{33} - C_{12} - C_{13} - C_{23}}{15} + \frac{C_{44} + C_{55} + C_{66}}{5} \tag{3}$$

and by Reuss that:

$$B_{\mathrm{R}} = \frac{1}{S_{11} + S_{22} + S_{33} + 2(S_{12} + S_{13} + S_{23})} \tag{4}$$

$$G_{\mathrm{R}} = \frac{15}{4(S_{11} + S_{22} + S_{33}) + 3(S_{44} + S_{55} + S_{66}) - 4(S_{12} + S_{13} + S_{23})} \tag{5}$$

The bulk modulus and shear modulus can be obtained by the Voigt-Reuss-Hill method. The arithmetic average of Voigt and Reuss bounds is known as the Voigt-Reuss-Hill average, which is regarded as the best estimate for the theoretical value of polycrystalline elastic modulus:

$$B = \frac{B_{\mathrm{V}} + B_{\mathrm{R}}}{2} \tag{6}$$

$$G = \frac{G_{\mathrm{V}} + G_{\mathrm{R}}}{2} \tag{7}$$

The Young's modulus and Poisson's ratio can be computed based on the above values by:

$$E = \frac{9BG}{3B + G} \tag{8}$$

$$\mu = \frac{3B - 2G}{6B + 2G} \tag{9}$$

where *B, G*, *E*, and μ of $Al_{1-x}TM_xP$ are calculated according to eqs. (2)-(9). The calculation results are shown in fig. 2.

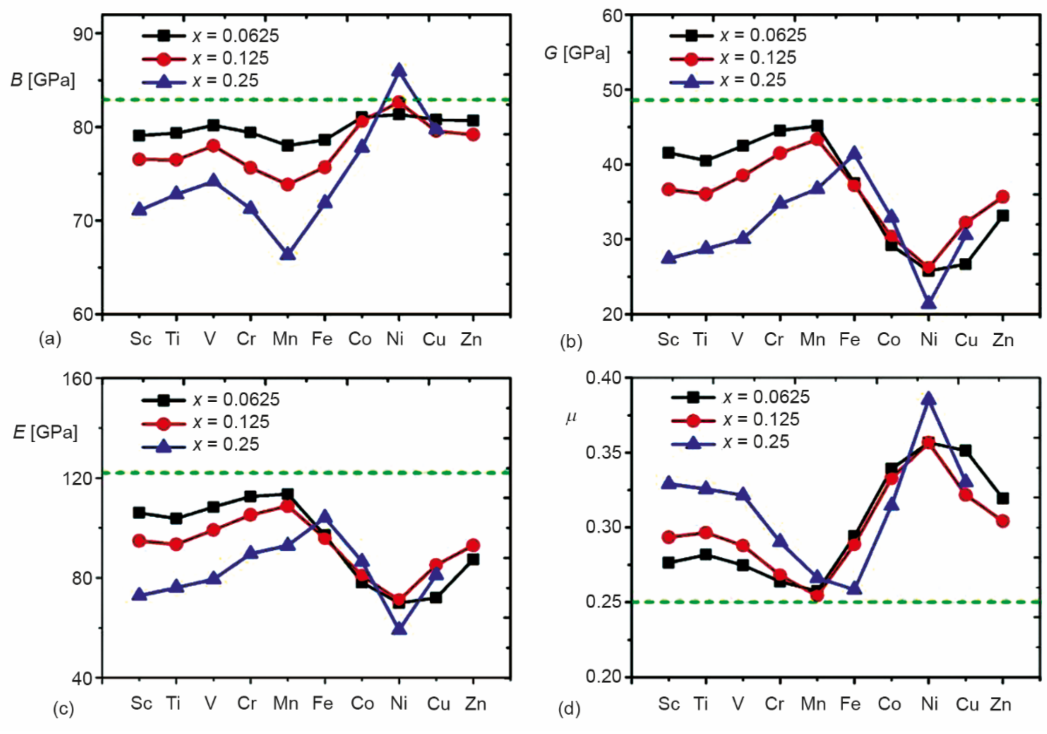

Figure 2. (a) The bulk modulus of $Al_{1-x}TM_xP$, (b) the shear modulus of $Al_{1-x}TM_xP$, (c) the Young's modulus of $Al_{1-x}TM_xP$, and (d) the Poisson's ration of $Al_{1-x}TM_xP$

The bulk modulus *B* of $Al_{1-x}TM_x$Pis shown in fig. 2(a). The dash line denotes the bulk modulus *B* of the pure AlP. After doping TM into AlP, except $Al_{0.75}Ni_{0.25}P$, the bulk modulus *B* of $Al_{1-x}TM_x$ is decreased. The bulk modulus of $Al_{0.75}Ni_{0.25}P$ is the largest (85.94 GPa) and the bulk modulus of $Al_{0.75}Mn_{0.25}P$ is the smallest (66.33 GPa).

The *G* of $Al_{1-x}TM_xP$ is shown in fig. 2(b). The dash line denotes the *G* of the pure AlP. After doping TM into AlP, the shear modulus *G* of $Al_{1-x}TM_x$ is decreased. The shear modulus of $Al_{0.9375}Mn_{0.0625}P$ is the largest (45.14 GPa) and the shear modulus of $Al_{0.75}Ni_{0.25}P$ is the smallest (21.34 GPa).

The Young's modulus *E* of $Al_{1-x}TM_xP$ is shown in fig. 2(c). The dash line denotes the Young's modulus *E* of the pure AlP. After doping TM into AlP, the Young's modulus of all $Al_{1-x}TM_xP$ is decreased. The Young's modulus of $Al_{0.9375}Mn_{0.0625}P$ is the largest (113.52 GPa) and the Young's modulus of $Al_{0.75}Ni_{0.25}P$ is the smallest (59.13 GPa).

The Poisson's ratio μ of $Al_{1-x}TM_xP$ is shown in fig. 2(d). The dash line denotes the Poisson's ratio μ of the pure AlP. After doping TM into AlP, the Poisson's ratio of all $Al_{1-x}TM_xP$ is decrease. The Poisson's ratio of $Al_{0.75}Ni_{0.25}P$ is the largest (0.39) and the Poisson's ratio of $Al_{0.875}Mn_{0.125}P$ is the smallest (0.25).

Vickers hardness and ductility

The hardness of a material is the intrinsic resistance to deformation when a force is applied. Currently, a formal theoretical definition of hardness is still a challenge for material scientists. The hardness of a material is related to the elastic and plastic properties, there have been some semi-empirical model developed to predict the hardness of materials. Chen *et al*. [26] proposed a model to predict the hardness of polycrystalline materials and bulk metallic glassed based on the Pugh's modulus ration ($k = G/B$) and the shear modulus:

$$H_{\mathrm{V}} = 1.887k^{1.171}G^{0.591} \tag{10}$$

where H_{V} denotes the Vickers hardness.

The ration of B/G can be used to estimate the ductility or brittleness of materials [27], since a high (low) value is associated with ductility(brittleness), and the critical value is about 1.75.

$$D = \frac{B}{G} \tag{11}$$

The H_{V} and B/G of $Al_{1-x}TM_xP$ are calculated according to eqs. (10) and (11). The calculation results are shown in fig. 3.

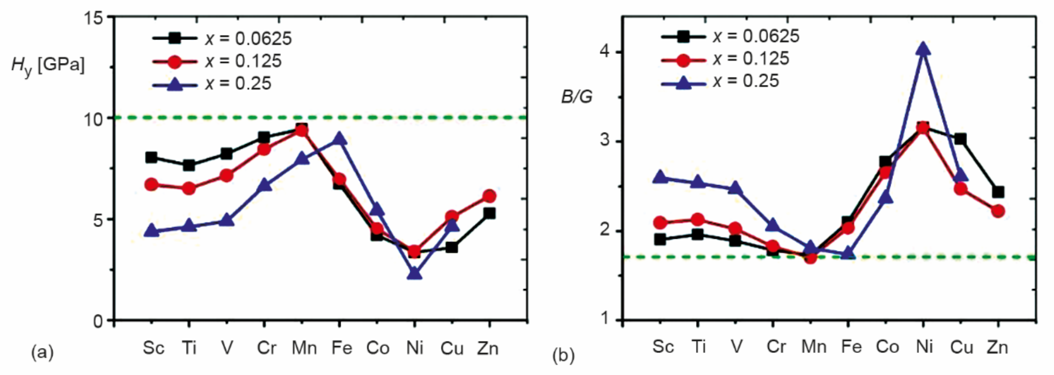

Figure 3. (a) The H_{V} of $Al_{1-x}TM_xP$ and (b) the B/G of $Al_{1-x}TM_xP$

The Vickers hardness H_{V} of $Al_{1-x}TM_xP$ is shown in fig. 3(a). The dash line denotes the Vickers hardness H_{V} of the pure AlP. After doping TM into AlP, the Vickers hardness of all $Al_{1-x}TM_xP$ are decreases. The Vickers hardness of $Al_{0.9375}Mn_{0.0625}P$ is the largest (9.45 GPa) and the Vickers hardness of $Al_{0.75}Ni_{0.25}P$ is the smallest (2.25 GPa).

The B/G of $Al_{1-x}TM_xP$ is shown in fig. 3(b). The dash line denotes the B/G of the pure AlP. After doping TM into AlP, the ductility of all $Al_{1-x}TM_xP$ are creases. The ductility of $Al_{0.75}Ni_{0.25}P$ is the largest (4.03) and the ductility of $Al_{0.875}Mn_{0.125}P$ is the smallest (1.70).

Elastic anisotropy

Several methods have been developed [27] to estimate he elastic anisotropy of compound. The bulk modulus anisotropy, A_{B}, shear modulus anisotropy, A_{G}, Young's modulus anisotropy, A_E, universal elastic anisotropy index, A_U, and for a crystal with orthorhombic symmetry can be determined:

$$A_B = \frac{B_V - B_R}{B_V + B_R}$$
$$A_G = \frac{G_V - G_R}{G_V + G_R}$$
$$A_E = \frac{E_V - E_R}{E_V + E_R} \tag{12}$$
$$A_U = 5\frac{G_V}{G_R} + \frac{B_V}{B_R} - 6$$

Similar to the definitions of B_V, B_R, G_V, and G_R, E_V and E_R are the lower and upper bounds of Young's modulus in the in the Voigt and Reuss approximations, respectively. E_V and E_R are different from B_V, B_R, G_V, and G_R. they have no analytical solution and can only obtain numerical solution. The 3-D surface constructions of Young's modulus, E, for orthorhombic system is calculated by [27]:

$$\frac{1}{E} = S_{11}l_1^4 + S_{22}l_2^4 + S_{33}l_3^4 + (2S_{12} + S_{66})l_1^2l_2^2 + (2S_{13} + S_{55})l_1^2l_3^2 + (2S_{23} + S_{44})l_2^2l_3^2 \tag{13}$$

According to eq. (13), the value of Young's modulus, E, along any direction in 3-D space can be obtained, and its maximum value, E_V, and minimum values, E_R, can be further obtained.

The zero value of anisotropic index (A_B, A_G, A_E, A_U) indicates that the crystal is isotropic. A high value of anisotropic index (A_B, A_G, A_E, A_U) means that the crystal structure has highly anisotropic elastic properties. The A_B, A_G, A_E and A_U of $Al_{1-x}TM_xP$ are calculated according to eqs. (12) and (13). The calculation results are shown in fig. 4.

The bulk modulus anisotropy A_B of $Al_{1-x}TM_xP$ is shown in fig. 4(a). The dash line denotes the A_B of the pure AlP. After doping TM into AlP, the bulk modulus anisotropy of $Al_{1-x}TM_xP$ are increased slightly. The bulk modulus anisotropy of $Al_{1-x}TM_xP$ is very small, almost approach zero. The bulk modulus anisotropy of $Al_{0.75}Cu_{0.25}P$ is the largest (2.39%).

The A_G of $Al_{1-x}TM_xP$ is shown in fig. 4(b). The dash line denotes the A_G of the pure AlP. After doping TM into AlP, the shear modulus anisotropy of $Al_{1-x}TM_xP$ are decreases except for $Al_{0.75}Ni_{0.25}P$ and $Al_{0.75}Cu_{0.25}P$. The shear modulus anisotropy of $Al_{0.75}Cu_{0.25}P$ is the largest (31.33%) and the shear modulus anisotropy of $Al_{0.75}Sc_{0.25}P$ is the smallest (2.29%).

The A_E of $Al_{1-x}TM_xP$ is shown in fig. 4(c). The dash line denotes the A_E of the pure AlP. After doping TM into AlP, the Young's modulus anisotropy of most $Al_{1-x}TM_xP$ are creases. The Young's modulus anisotropy of $Al_{0.75}Cu_{0.25}P$ is the largest (69.94%) and the Young's modulus anisotropy of $Al_{0.75}Sc_{0.25}P$ is the smallest (22.15%).

The A_U of $Al_{1-x}TM_xP$ is shown in fig. 4(d). The dash line denotes the A_U of the pure AlP. After doping TM into AlP, the universal elastic anisotropy index of most $Al_{1-x}TM_xP$ are creases. The universal elastic anisotropy of $Al_{0.75}Cu_{0.25}P$ is the largest (4.61) and the universal elastic anisotropy of $Al_{0.75}Sc_{0.25}P$ is the smallest (0.24).

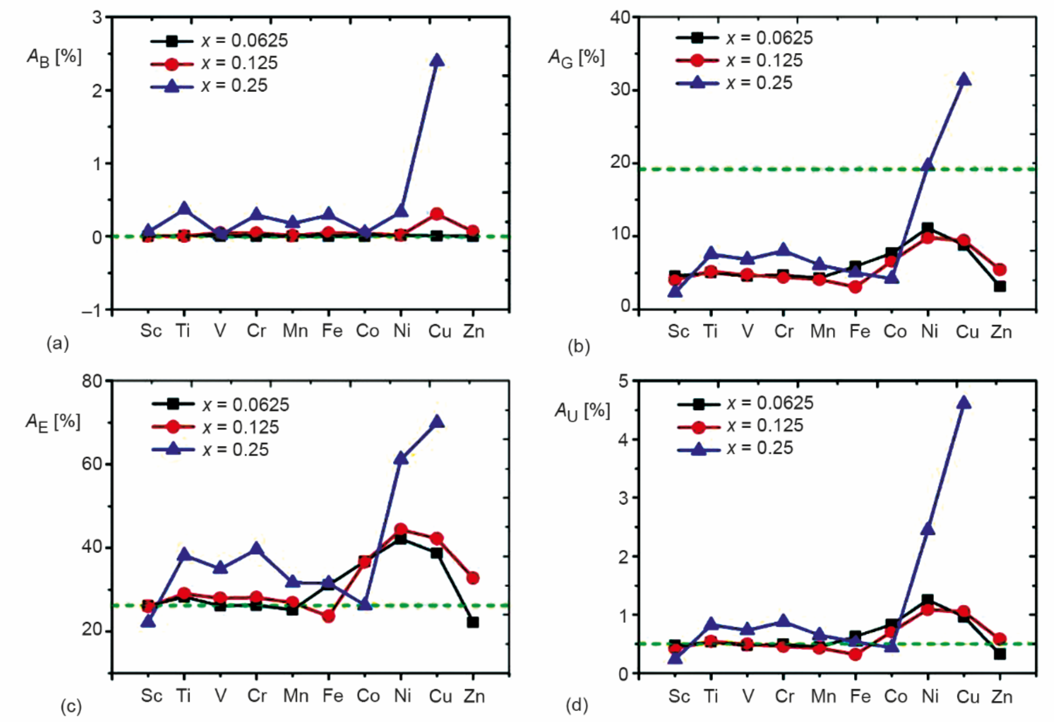

Figure 4. (a) The bulk modulus anisotropy factors of $Al_{1-x}TM_xP$, (b) the shear modulus anisotropy factors of $Al_{1-x}TM_xP$, and (c) the universal elastic anisotropy factors of $Al_{1-x}TM_xP$

Based on the comprehensive analysis of four elastic anisotropy factors, $Al_{0.75}Cu_{0.25}P$ has the largest elastic anisotropy value. Except $Al_{0.75}Ni_{0.25}P$ and $Al_{0.75}Cu_{0.25}P$, the elastic anisotropy of $Al_{1-x}TM_xP$ is insensitive to dope concentration.

Conclusion

In this work, based on the first-principles calculations, mechanical properties of $Al_{1-x}TM_xP$ (x = 0.0625, 0.125, 0.25; TM = Sc, Ti, V, Cr, Mn, Fe, Co, Ni, Cu, and Zn) crystal have studied in the orthorhombic phase. By analyzing the mechanical stability, it is found that $Al_{0.75}Zn_{0.25}P$ is mechanically unstable, and the rest all mechanically stable. It is found that $Al_{0.75}Ni_{0.25}P$ has the largest bulk modulus, the largest Poisson's ratio. $Al_{0.75}Ni_{0.25}P$ has the smallest shear modulus, the smallest Young's modulus and the smallest Vickers hardness. The $Al_{0.75}Ni_{0.25}P$ has the best ductility. $Al_{0.75}Ni_{0.25}P$ and $Al_{0.75}Cu_{0.25}P$ show strong elastic anisotropy, and the $Al_{0.75}Cu_{0.25}P$ has the largest elastic anisotropy. Through the study of the mechanical properties of $Al_{1-x}TM_xP$, it is found that doping Ni in AlP is an effective means to tune its mechanical properties. The present method can be extended to study the TM-doped nanofiber properties [28, 29] by the electrospinning technology or the bubble electrospinning [30-35].

Acknowledgment

The research work is supported by the Research Program of Science and Technology at Universities of Inner Mongolia Autonomous Region (NJZY22389), Basic Scientific Research Expenses Program of Universities directly under Inner Mongolia Autonomous Region (JY20220213) and the Scientific Research Project of Inner Mongolia University of Technology (BS2021058).

References

[1] Sun, J. P., Stability and Electronic Structures of Single-Walled Alp Nanotubes by First Principle Study, *Procedia Engineering, 15* (2011), Dec., pp. 5062-5066
[2] Yang, R., *et al.*, First-Principles Study on Phases of AlP, *Solid State Communications, 267* (2017), Nov., pp. 23-28
[3] Zhang, Y., Possible Room Temperature Ferromagnetism in Ca-doped AlP: First-Principles Study, *Journal of Magnetism and Magnetic Materials, 342* (2013), Sept., pp. 35-37
[4] Liang, P., *et al.*, The Half Metallic Property and Electronic Structure of the Ti Doped AlP Systems Investigated by First Principle, *Journal of Magnetism and Magnetic Materials, 355* (2014), Apr., pp. 295-299
[5] Kervan, S., Kervan, N., First-Principles Study on Half-Metallic Ferromagnetism in the Diluted Magnetic Semiconductor (DMS) $Al_{1-x}Mn_xP$ Compounds, *Journal of Magnetism and Magnetic Materials, 382* (2015), May, pp. 63-70
[6] Yan, Z., *et al.*, Ferromagnetism in Alkali-Metal-Doped AlP: An ab Initio Study, *Computational Materials Science, 99* (2015), Mar., pp. 16-20
[7] Lakel, S., *et al.*, Optical and Electronic Properties of $B_xAl_{1-x}P$ Alloys: A First Principles Study, *Optik 127* (2016), 8, pp. 3755-3761
[8] Wang, S., *et al.*, Room-Temperature Ferromagnetism in Alkaline-Earth-Metal Doped AlP: First-Principle Calculations, *Computational Materials Science, 142* (2018), Feb., pp. 338-345
[9] Liu, C., *et al.*, Two-Dimensional Tetragonal AlP Monolayer: Strain-Tunable Direct-Indirect Band-Gap and Semiconductor-Metal Transitions, *Journal of Materials Chemistry C, 24* (2017), 5, pp. 5999-6004
[10] Akbari, A., *et al.*, Tuning the Electronic and Optical Properties of XP (X = Al, Ga) Monolayer Semiconductors Using Biaxial Strain Effect: Modified Becke-Johnson Calculations, *Chemical Physics Letters, 691* (2018), Jan., pp. 181-189
[11] Chen, Y., *et al.*, Enhanced Optical Absorption in Visible Range in Mn Doped AlP: A Density Functional Theory Study, *Journal of Magnetism and Magnetic Materials, 457* (2018), July, pp. 13-16
[12] Zhang, Y., *et al.*, Half-Metallic Ferromagnetism in Cr-doped AlP-Density Functional Calculations, *Solid State Communications, 145* (2008), 11-12, pp. 590-593
[13] Sajjad, M., *et al.*, First Principles Study of Structural, Elastic, Electronic and Magnetic Properties of Mn-doped AlY (Y = N, P, As) Compounds, *Journal of Magnetism and Magnetic Materials, 390* (2015), Sept., pp. 78-86
[14] Togo, A., Tanaka, I., First Principles Phonon Calculations in Materials Science, *Scripta Materialia, 108* (2015), Nov., pp. 1-5
[15] Chettri, B., *et al.*, First Principle Insight into Co-doped MoS_2 for Sensing NH_3 and CH_4, *Facta Universitatis Series: Mechanical Engineering, 35* (2022), 1, pp. 43-59
[16] Chen, G. Y., *et al.*, First-Principles Study of Calcium-Based Sulfur Fixers and Their Products, *Thermal Science, 26* (2022), 5A, pp. 3843-3857
[17] Grimme, S., *et al.*, Effect of the Damping Function in Dispersion Corrected Density Functional Theory, *Journal of Computational Chemstry, 32* (2011), 7, pp. 1456-1465
[18] Segall, M. D., *et al.*, First-Principles Simulation: Ideas, Illustrations and the CASTEP Code, *Journal of Physics-Condensed Matter, 14* (2002), 11, pp. 2717-2744
[19] Clark, S. J., *et al.*, First Principles Methods Using CASTEP, *Zeitschrift fur Kristallographie, 220* (2005), 5-6, pp. 567-570
[20] Perdew, J. P., *et al.*, Generalized Gradient Approximation Made Simple, *Physical Review Letters, 77* (1996), 18, pp. 3865-3868
[21] Ernzerhof, M., Scuseria, G. E., Assessment of the Perdew-Burke-Ernzerhof Exchange-Correlation Functional, *Journal of Chemical Physics, 110* (1999), 11, pp. 5029-5036
[22] Wu, Z., *et al.*, Crystal stRuctures and Elastic Properties of Superhard IrN_2 and IrN_3 from First Principles, *Physical Review B, 76* (2007), Aug., pp. 054115 (1)-054115 (15)
[23] Mouhat, F., Coudert F., Necessary and Sufficient Elastic Stability Conditions in Various Crystal Systems, *Physical Review B, 90* (2014), Dec., pp. 224104 (1)-224104 (4)

[24] Li, L., *et al*., First-Principle Calculations of Structural, Elastic and Thermodynamic Properties of Fe-B Compounds, *Intermetallics*, *46* (2014), Mar., pp. 211-221
[25] Li, L. H., *et al*., First-Principle and Molecular Dynamics Calculations for Physical Properties of Ni-Sn Alloy System, *Computational Materials Science*, *99* (2015), Mar., pp. 274-284
[26] Chen, X.-Q., *et al*., Modeling Hardness of Polycrystalline Materials and Bulk Metallic Glasses, *Intermetallics*, *19* (2011), 9, pp. 1275-1281
[27] Shao, P., *et al*., Structural, Electronic and Elastic Properties of the Shape Memory Alloy NbRu: First-Principle Investigations, *Journal of Alloys and Compounds*, *695* (2017), Feb., pp. 3024-3029
[28] Li, Y., *et al*., Ultrafine and Polar ZrO_2-inlaid Porous Nitrogen-Doped Carbon Nanofiber as Efficient Polysulfide Absorbent For High-Performance Lithium-Sulfur Batteries with Long Lifespan, *Chemical Engineering Journal*, *349* (2018), Oct., pp. 376-387
[29] Chen, M. Y., *et al*., Nanofiber Template-Induced Preparation of ZnO Nanocrystal and Its Application in Photocatalysis, *Scientific Reports*, *11* (2021), Oct., 21196
[30] He, C. H., *et al*., Taylor Series Solution for fractal Bratu-type Equation Arising in Electrospinning Process, *Fractals*, *28* (2020), 1, 2050011
[31] He, J.-H., *et al*., The Maximal Wrinkle Angle During the Bubble Collapse and Its Application to the Bubble Electrospinning, *Frontiers in Materials*, *8* (2022), 800567
[32] Qian, M. Y., He, J.-H., Collection of Polymer Bubble as a Nanoscale Membrane, *Surfaces and Interface*, *28* (2022), 101665
[33] Zuo, Y. T., Liu, H. J., Is the Spider a Weaving Master or a Printing Expert? *Thermal Science*, *26* (2022) , 3B, pp. 2471-2475
[34] Liu, H. Y., *et al*., Interaction of Multiple Jets in Bubble Electrospinning, *Thermal Science*, *27* (2023), 3A, pp. 1741-1746
[35] Li, X. X., *et al*., Temperature-Dependent Capillary Rise and Its Effects on Fabric Cleaning and Permeability, *Thermal Science*, *27* (2023), 3A, pp. 1915-1920

Paper submitted: January 14, 2023
Paper revised: August 1, 2023
Paper accepted: August 5, 2023